Supplement of Atmos. Chem. Phys., 16, 8729–8747, 2016
http://www.atmos-chem-phys.net/16/8729/2016/
doi:10.5194/acp-16-8729-2016-supplement

Atmospheric Chemistry and Physics Open Access EGU

Supplement of

Model–measurement comparison of functional group abundance in α-pinene and 1,3,5-trimethylbenzene secondary organic aerosol formation

G. Ruggeri et al.

Correspondence to: Satoshi Takahama (satoshi.takahama@epfl.ch)

This document contains Appendices S1 and S2 as well as supplemental figures S1–S14.

S1 Dynamic absorptive partitioning

In this section, we summarize the dynamic absorptive partitioning batch reactor model (inspired by the continuous flow reactor model of Chen et al., 2011) and also our use of pure component and saturation concentrations. Symbols and their descriptions are listed in Table S1.

We first revisit the relationship among equilibrium vapor pressure p of a substance i in a mixture, its pure component vapor pressure (possibly over sub-cooled liquid) p^0, and its activity a of solution. The vapor and aerosol solution phase chemical potentials can be written as a sum of their standard chemical potentials μ^0 and μ^* and their ideal (and non-ideal, in the case of liquid) mixing contributions to the partial molar Gibbs free energy (Denbigh, 1981; Seinfeld and Pandis, 2006):

$$\mu_i^{(\text{vap.})} = \mu_i^0 + RT \ln p_i \tag{S1}$$

$$\mu_i^{(\text{soln.})} = \mu_i^* + RT \ln a_i \ . \tag{S2}$$

At equilibrium, the chemical potential of substance i in the two phases are equal, $\mu_i^{(\text{vap.})} = \mu_i^{(\text{soln.})}$; the equilibrium constant K is given by the relation between equations S1 and S2:

$$K_i = \exp\left(\frac{\mu_i^* - \mu_i^0}{RT}\right) = \frac{p_i}{a_i} \ . \tag{S3}$$

Using a pure component reference (as opposed to infinite dilution) for all species, $K_i = p_{L,i}^0$. With activity of substance i defined as $a_i = \zeta_i x_i$, the equality in equation S3 is commonly written as:

$$p_i = \zeta_i x_i p_{L,i}^0 \ . \tag{S4}$$

The pure component and equilibrium vapor pressures are equivalent to their mass concentrations C^0 and $C^{(\text{g})}$, respectively at a given temperature by the ideal gas law (Chen et al., 2011; Donahue et al., 2012):

$$C_i^0 = \frac{MW_i}{RT} p_{L,i}^0 \quad \text{and} \quad C_i^{(g)} = \frac{MW_i}{RT} p_i \ . \tag{S5}$$

Table S1. Summary of variables and notation used for model description.

Symbol	Description
i	compound index
n	number of moles
x	mole fraction in solution
μ	chemical potential ($\mathrm{kJ\,mol^{-1}}$)
μ^0	standard chemical potential (gas-phase reference at 1 atm, $\mathrm{kJ\,mol^{-1}}$)
μ^*	standard chemical potential (liquid-phase reference, $\mathrm{kJ\,mol^{-1}}$)
K	equilibrium constant
a	solution activity
ζ	activity coefficient
p	equilibrium vapor pressure (atm)
p_L^0	pure component vapor pressure (atm)
$C^{(\mathrm{g})}$	gas-phase concentration ($\mu\mathrm{g\,m^{-3}}$)
$C^{(\mathrm{p})}$	particle-phase concentration ($\mu\mathrm{g\,m^{-3}}$)
C^0	pure component concentration ($\mu\mathrm{g\,m^{-3}}$)
C^*	saturation concentration ($\mu\mathrm{g\,m^{-3}}$)
C_{OA}	organic aerosol concentration ($\mu\mathrm{g\,m^{-3}}$)
MW	molecular weight ($\mathrm{g\,mol^{-1}}$)
$\overline{MW}$	mean molecular weight ($\mathrm{g\,mol^{-1}}$)
R	gas constant ($\mathrm{m^3 atm\,K^{-1}\,mol^{-1}}$)
T	temperature (K)
K_p	partitioning coefficient ($\mathrm{m^3\,\mu g^{-1}}$)
D_p	particle diameter (nm)
D_{seed}	seed diameter (nm)
D	diffusivity ($\mathrm{m^2 s^{-1}}$)
N_p	number concentration ($\mathrm{m^{-3}}$)
ρ_p	SOA density ($\mathrm{g\,cm^{-3}}$)
Kn	Knudsen number
λ	mean free path (m)

The saturation concentration C^* (Donahue et al., 2006) is also a widely used metric for characterizing the volatility of a mixture; it is the reciprocal of the venerable G/P partition coefficient K_p (Pankow, 1994, 2011):

$$C_i^* = \frac{C_i^{(g)}}{C_i^{(p)}} C_{\mathrm{OA}} = \left(\frac{C_i^{(p)}}{C_{\mathrm{OA}}} \right)^{-1} C_i^{(g)} = K_{p,i}^{-1} \, . \tag{S6}$$

The mass fraction of i in the particle phase (with respect to the total organic aerosol mass) can be expressed according to its molar abundance n, mole fraction x, and molecular weight MW , and the mean molecular weight $\overline{MW}$ defined for the set of compounds $\mathcal{M}$ in the mixture:

$$\frac{C_i^{(p)}}{C_{\mathrm{OA}}} = \frac{MW_i n_i}{\sum_{i\in\mathcal{M}} MW_i n_i} = \frac{MW_i}{\overline{MW}} \cdot \frac{n_i}{\sum_{i\in\mathcal{M}} n_i} = \frac{MW_i}{\overline{MW}} x_i \,. \tag{S7}$$

By substitution of equation S7 into S4–S6, C_i^* can be related to C_i^0:

$$C_i^* = \frac{\overline{MW}}{RT}\frac{p_i}{x_i} = \frac{\overline{MW}}{RT}\zeta_i p_{L,i}^0 = \frac{\overline{MW}}{MW_i}\zeta_i C_i^0 \tag{S8}$$

For a pure component solution, $C_i^* = C_i^0$. At equilibrium with a solution mixture, the gas phase concentration is related to saturation concentrations C_i^0 and C_i^* through equations S4–S6:

$$C_i^{(\mathrm{g})} = a_i C_i^0 = \frac{C_i^{(p)}}{C_{\mathrm{OA}}} C_i^*$$

C^* is a useful construct to represent volatility of aggregated mixtures when its composition is not well-defined (Donahue et al., 2006; Grieshop et al., 2009; Chen et al., 2011), and we use this for specifying initial concentrations of a generic organic aerosol mixture (Appendix S2). For subsequent G/P partitioning calculations, we follow the approach of Donahue et al. (2012) and use C^0 according to molecular specificity provided by the MCMv3.2 mechanism.

Considering the dynamics of condensation and evaporation, mass transfer of individual compounds from the bulk vapor phase (at concentration $C_{i,\infty}^{(\mathrm{g})}$) to a monodisperse particle population of size D_p is driven by the concentration gradient with respect to the equilibrium vapor concentration at the aerosol surface, and the surface characteristics for exchange to take place (Fuchs and Sutugin, 1971; Seinfeld and Pandis, 2006; Chen et al., 2011):

$$\frac{dC_{i,\infty}^{(\mathrm{g})}}{dt} = -\frac{dC_i^{(p)}}{dt} = -2\pi N_p D_p D_i f(\alpha_i, Kn)(C_{i,\infty}^{(\mathrm{g})} - a_i C_i^0) \tag{S9}$$

$$f(\alpha_i, Kn) = \frac{0.75\alpha_i(1+Kn)}{Kn^2 + Kn + 0.283 Kn\alpha_i + 0.75\alpha_i}$$

We assume activity coefficients ζ_i and mass accommodations α_i of unity, and a diffusivity of $D_i = 5\times10^{-6}\ \mathrm{m^2\,s^{-1}}$ for all molecules (Chen et al., 2011). One notable difference with Chen et al. (2011) is that we run this model as a batch reactor rather than a continuously-stirred flow tank reactor, in accordance with the operation of experimental chambers of the reference studies used in this work.

Given our assumption of monodisperse particles and fixed particle number N_p (no particle losses; negligible coagulation for the duration of our simulations), we estimate the size D_p of particles (which includes the seed, if applicable, and condensed organic matter) at each timestep to satisfy the following condition, assuming SOA density of $\rho_p = 1.5\ \mathrm{g\,cm^{-3}}$ (Kostenidou et al., 2007):

$$C_{\mathrm{OA}} = N_p \rho_p \frac{\pi}{6}\left(D_p^3 - D_{\mathrm{seed}}^3\right)$$

Values for these parameters are discussed in Appendix S2.

S2 Initial and fixed conditions

In addition to precursor, NO_x , and oxidant concentrations specified in Table 1, we initialize gas-phase concentrations to small, non-zero values ($C_i^{(g)}$ set equivalent to 10^{-5} ppb for each compound) to prevent numerical singularities. The initial concentration of the aerosol phase is important also as it determines the activity (i.e., mole fraction) in equation S9. Assuming values at either extreme of the domain can lead to undesired behavior. In the perfect sink assumption (all $x_i = 0$), excess condensation of the most abundant gas-phase product (without regard to compound-specific saturation concentration) can occur in a single time step. In the pure component or external mixture assumption (all $x_i = 1$), condensation during initial stages can be extremely slow for simulations under low precursor concentrations, and erratic changes in equilibrium concentrations can occur when transitioning from $x_i = 1$ to $x_i \ll 1$ immediately following initial condensation.

The use of an organic seed aerosol ($C_{\text{OA,init}}$) to initiate G/P partitioning alleviates such problems and accounts for the effects of homogeneous and heterogeneous nucleation (Flagan and Seinfeld, 1988; Seinfeld and Pandis, 2006; Fan et al., 2013, e.g.,) of organic aerosol not included in our model. Pankow (2001) used $C_{\text{OA,init}}$ and composition (x_is) from the final C_{OA} values determined from experiments. As this can introduce additional mass into the system, we introduce a different approach. Initial aerosol concentrations are specified to be in equilibrium with the specified gas-phase concentrations for a given $C_{\text{OA,init}}$ (according to equations S6 and S8 with $\zeta_i = 1$):

$$C_i^{(p)} = \left(\frac{C_i^{(g)}}{C_i^*}\right) C_{\text{OA,init}} = \left(\frac{C_i^{(g)}}{C_i^0} \cdot \frac{MW_i}{\overline{MW}}\right) C_{\text{OA,init}} \ . \tag{S10}$$

This leads to the introduction of negligible mass of MCM compounds into the system, but provides a means for determining non-zero initial values of x_is that scale with the vapor pressures of condensible products. For typical values of $C_{\text{OA,init}}$, $\sum_{i\in\mathcal{M}'} C_i^{(p)} \ll C_{\text{OA,init}}$ where $\mathcal{M}'$ represents all compounds in the MCM mechanism; we assume the existence of an inactive medium (C_{solvent}) which comprises this difference:

$$C_{\text{solvent}} = C_{\text{OA,init}} - \sum_{i\in\mathcal{M}'} C_i^{(p)} \ .$$

C_{solvent} does not participate in G/P partitioning or reactions, and is not reported with the SOA formed. The initial and subsequent mole fractions are calculated in the presence of this virtual medium:

$$x_i = \frac{C_i^{(p)}/MW_i}{\sum_{i\in\mathcal{M}'} C_i^{(p)}/MW_i + C_{\text{solvent}}/\overline{MW}_{\text{solvent}}} \ . \tag{S11}$$

$\mathcal{M}'$, in combination with this inactive medium, comprises the complete set of molecule types $\mathcal{M}$ in the system (Appendix S1).

A value of $C_{\text{OA,init}} = 1\ \mu\text{g}\,\text{m}^{-3}$ is assumed in all of our simulations, which leads to initial values of $\sum_i C_i^{(p)} < 5 \times 10^{-4}$ $\mu\text{g}\,\text{m}^{-3}$. Therefore, $C_{\text{solvent}} \sim C_{\text{OA,init}}$ and the organic aerosol phase affecting G/P partitioning is effectively $C_{\text{OA}} = C_{\text{solvent}} + C_{\text{SOA}} \approx C_{\text{OA,init}} + C_{\text{SOA}}$. For use in both equations S10 and S11 we assume a mean molecular weight of $\overline{MW} = \overline{MW}_{\text{solvent}} = 200\ \text{g}\,\text{mol}^{-1}$, which is in the range of products estimated or identified in the condensed phase (e.g., Odum et al., 1996; Nguyen et al., 2010; Shiraiwa et al., 2014). While C_{SOA} is several orders of magnitude greater than $C_{\text{OA,init}} = 1\ \mu\text{g}\,\text{m}^{-3}$ for APIN-lNO_x and TMB-lNO_x simulations (and therefore dominates x_is), C_{SOA} produced for APIN-hNO_x and APIN-nNO_x is within

the same order of magnitude for conceivable values of $C_{\text{OA,init}}$ near unity. However, in Figures S3 and S4 we illustrate that relative abundances of FGs analyzed reported in this work are relatively insensitive to the value of $C_{\text{OA,init}}$ and C_{SOA} for these latter simulations.

For experiments with ammonium sulfate seed (APIN-hNO$_x$ and APIN-nNO$_x$), we assume $D_{\text{seed}} = 200$ nm and $N_p = 3.5{\times}10^3\ \text{cm}^{-3}$, which corresponds to approximately 26 $\mu\text{g}\,\text{m}^{-3}$ of ammonium sulfate in accordance with experiments (Table 1). With $C_{\text{OA,init}} = 1\mu\text{g}\,\text{m}^{-3}$ and $\rho_p = 1.5\ \text{g}\,\text{cm}^{-3}$, initial D_p becomes 203 nm. For APIN-lNO$_x$ and TMB-lNO$_x$ where no seed is used, we assume $N_p = 10^4\ \text{cm}^{-3}$ and initial $D_p = 43$ nm is calculated according to $C_{\text{OA,init}}$, which corresponds to a system which condensational growth and scavenging of the smallest clusters has occured. The Kelvin effect is neglected but results are insensitive to this omission since the condensation and particle growth is rapid in these two systems. D_p increases up to 350 nm over the course of the APIN-lNO$_x$ and TMB-lNO$_x$ simulations for the given C_{OA} loadings, and up to 220 nm (including seed) for APIN-hNO$_x$ and APIN-nNO$_x$ on account of the lower mass loading. Inorganic reactions (such as the production of nitric acid) in simulations involving NO$_x$ are included to maintain radical balance, but are not treated in G/P partitioning. Rate of particle growth may therefore be underestimated when condensation of such species (e.g., nitric acid) may be important compared to the growth due to the organic phase.

Sensitivity of the rate of mass transfer (equation S9) to N_p, D_p, $\overline{MW}_{\text{solvent}}$ described above can be interpreted through the sensitivity to $C_{\text{OA,init}}$ as demonstrated for the APIN-hNO$_x$ and APIN-nNO$_x$ simulations. However, the chemistry of the gas phase and formation of condensible products is not affected significantly as the mass removed to the aerosol fraction (where they are shielded from further chemical reaction in our model) is generally small (Figure S12). Therefore, the relative composition of the gas and aerosol phases analyzed in this work are not changed significantly by these parameters in our simulations.

Supplemental figures

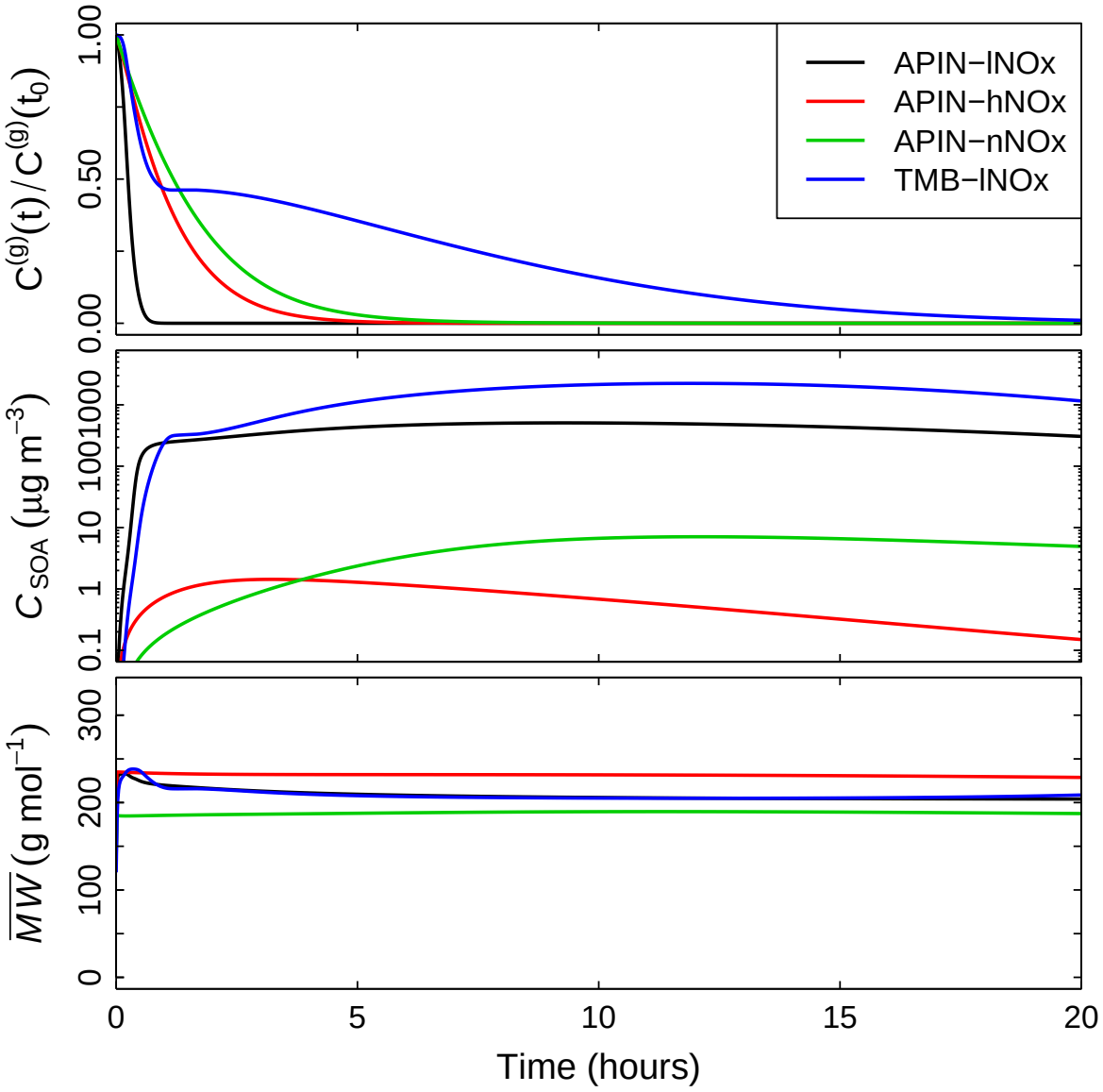

Figure S1. Time series of precursor concentrations ratioed to initial value (top), C_{SOA} ($= C_{\mathrm{OA}} - C_{\mathrm{OA,init}}$) concentrations (middle), and mean molecular weight of compounds weighted by abundance in the aerosol phase (bottom).

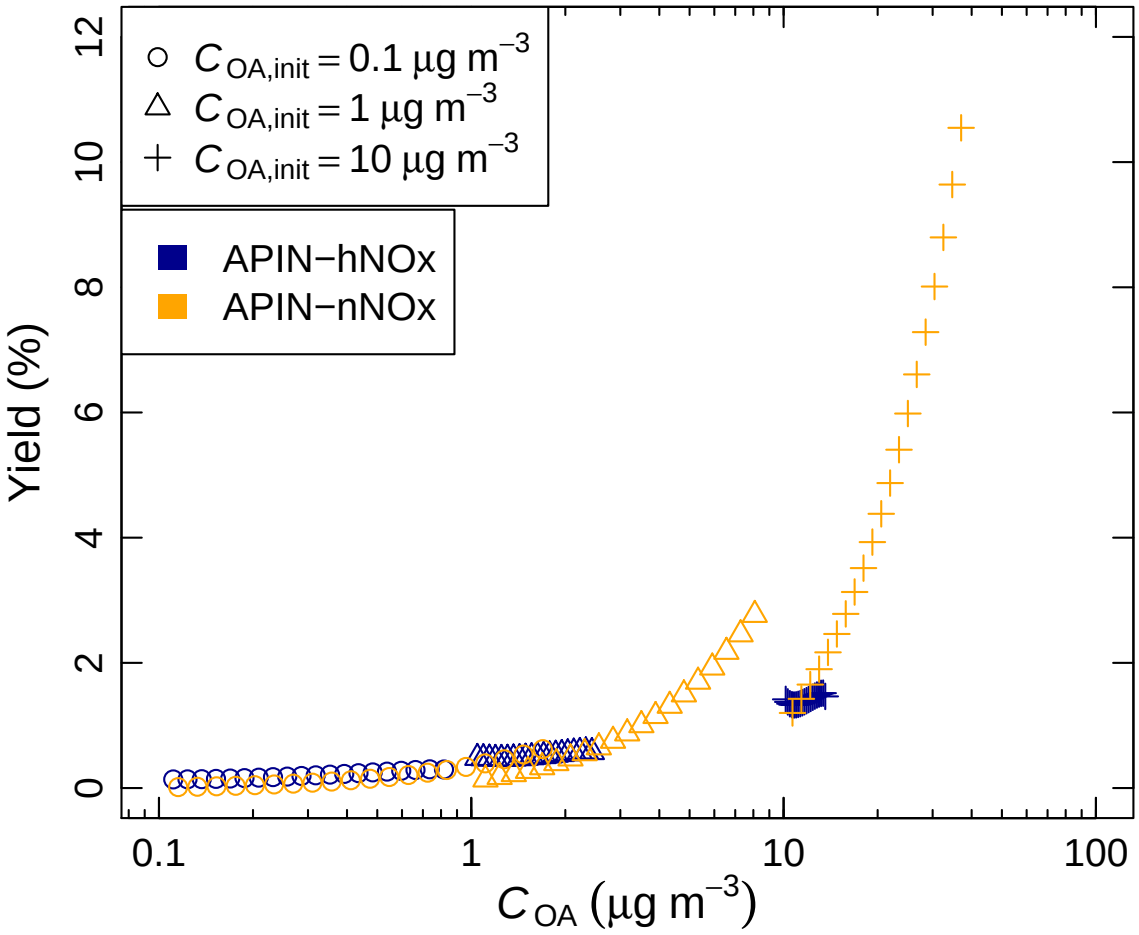

Figure S2. Aerosol yield curves for various values of $C_{\mathrm{OA,init}}$ in the APIN-hNO$_x$ and APIN-nNO$_x$ simulations. C_{OA} ($= C_{\mathrm{OA,init}} + C_{\mathrm{SOA}}$), which includes the SOA formed and $C_{\mathrm{OA,init}}$ to initiate G/P partitioning.

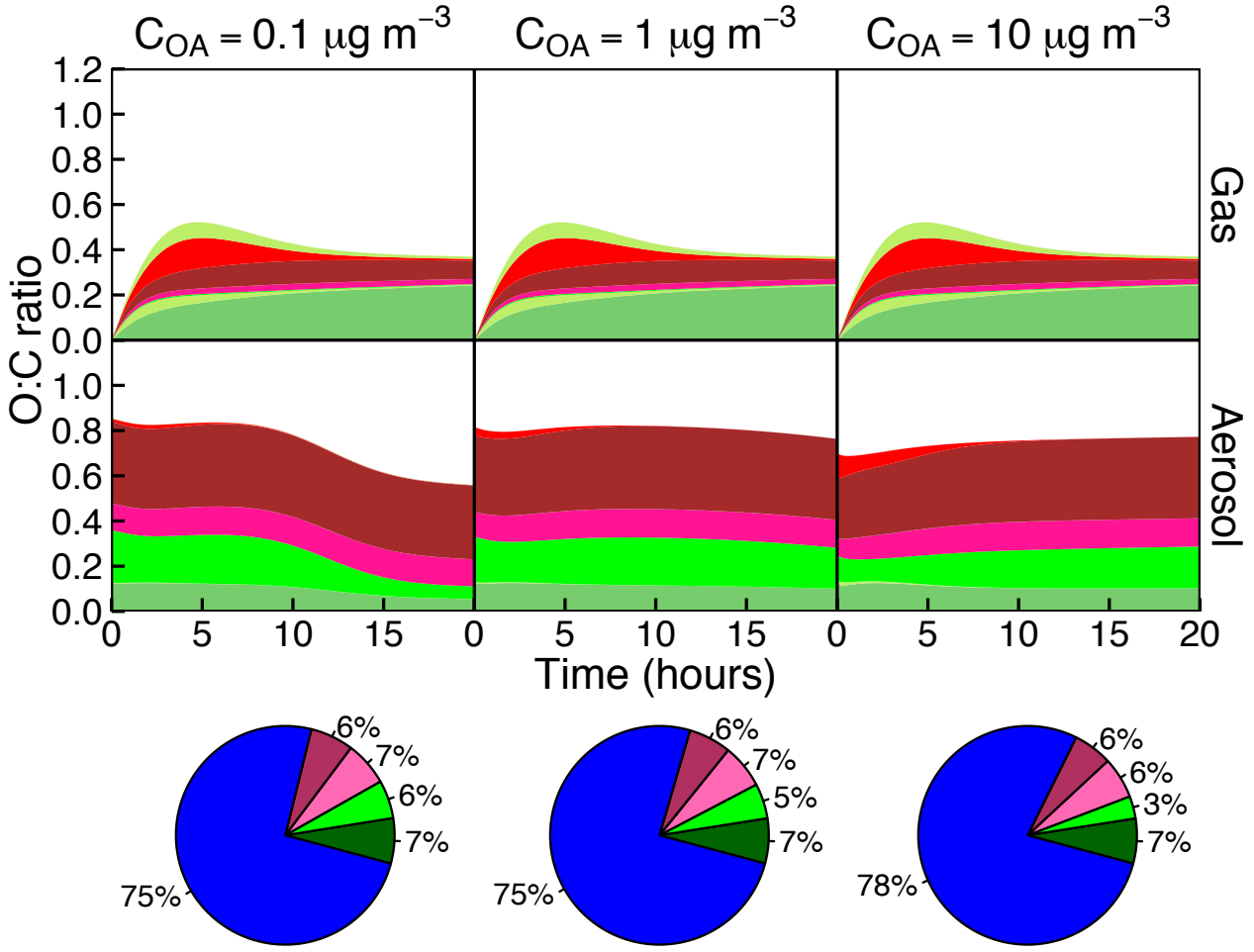

Figure S3. Evolution of O:C ratio for various values of $C_{OA,init}$ in the APIN-hNO$_x$ simulation. Color schemes are same as for Figures 1 and 3. Pie charts illustrate time-integrated composition for the first 8 hours.

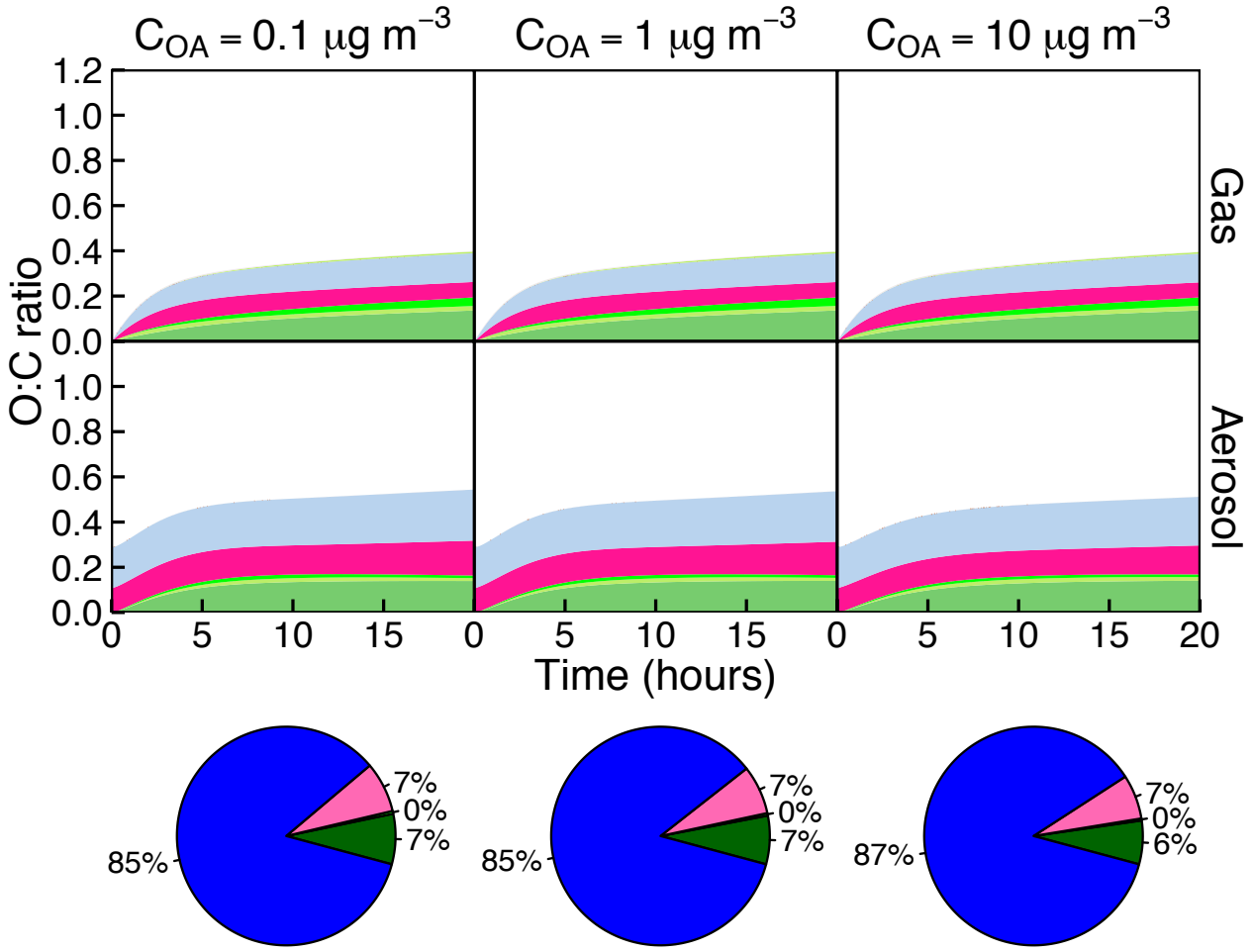

Figure S4. Evolution of O:C ratio for various values of $C_{OA,init}$ in the APIN-nNO$_x$ simulation. Color schemes are same as for Figures 1 and 3. Pie charts illustrate time-integrated composition for the first 8 hours.

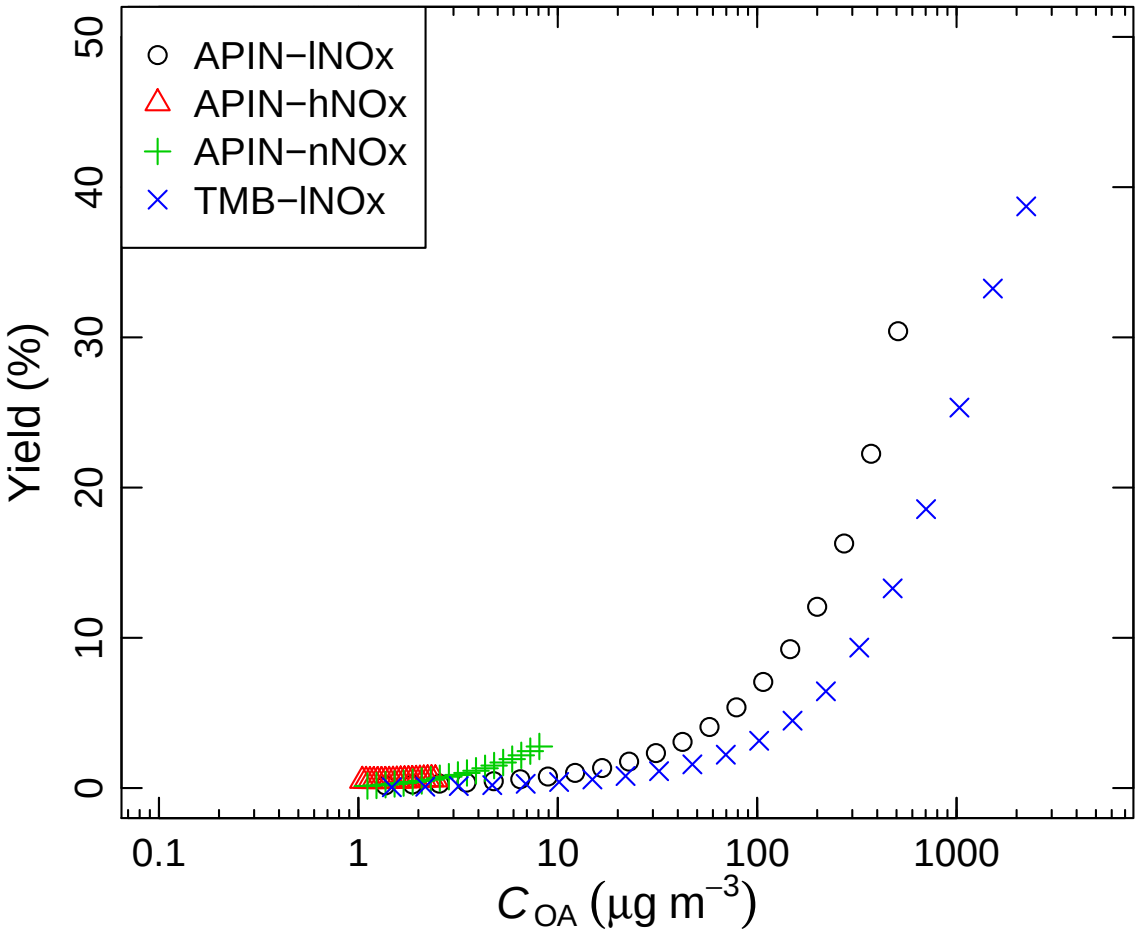

Figure S5. Aerosol yields ($C_{\mathrm{OA,init}}$ =1 µg m^{-3}) as a function of C_{OA} ($= C_{\mathrm{OA,init}} + C_{\mathrm{SOA}}$), which includes the SOA formed and $C_{\mathrm{OA,init}}$ to initiate G/P partitioning.

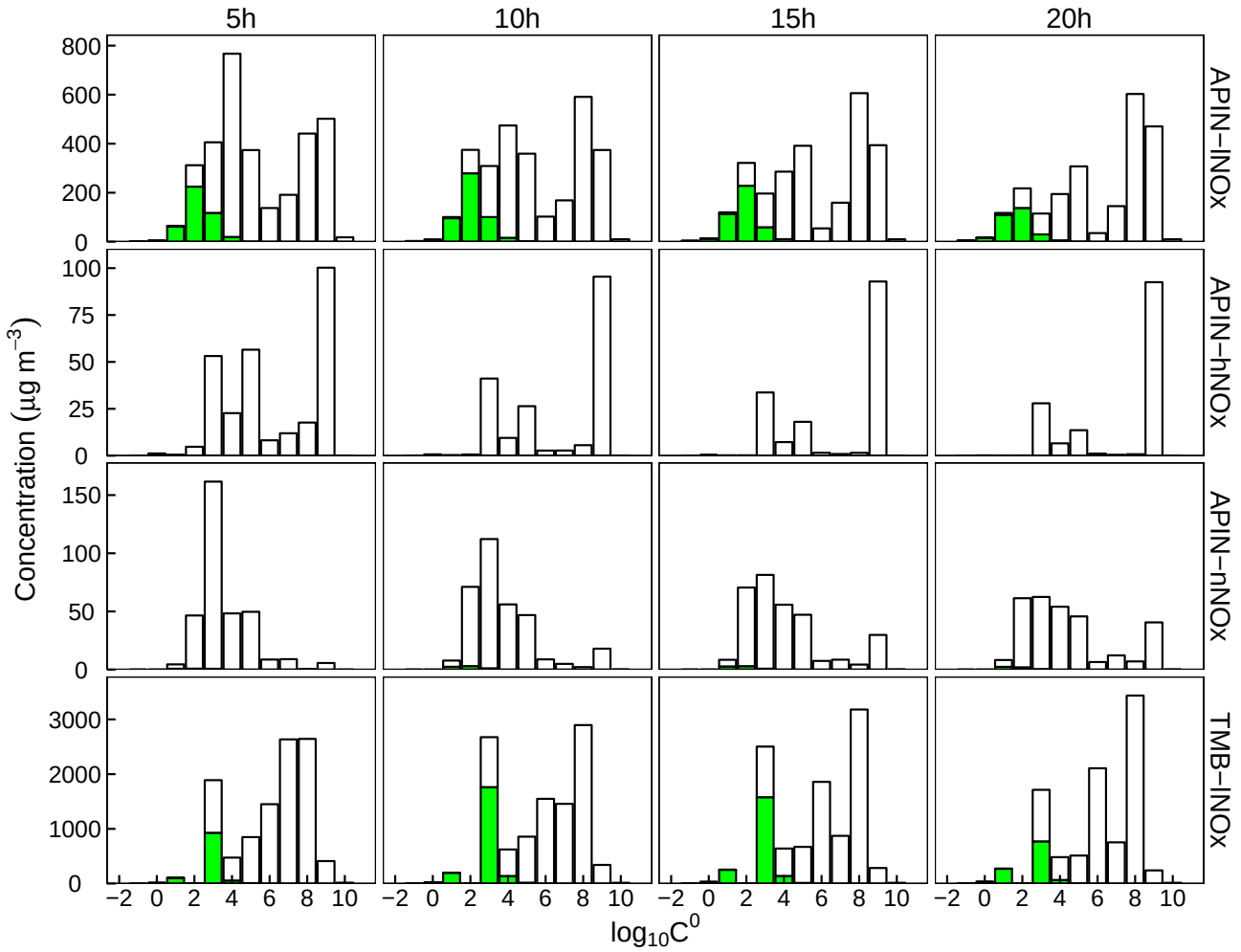

Figure S6. Volatility distribution of gas (white) and aerosol (green) phase products at different time intervals of the photooxidation simulation ($C_{\mathrm{OA,init}} = 1\,\mu\mathrm{g\,m^{-3}}$). C^0 is in units of $\mu\mathrm{g\,m^{-3}}$. Different simulations are shown in different rows with varying scales along y-axis.

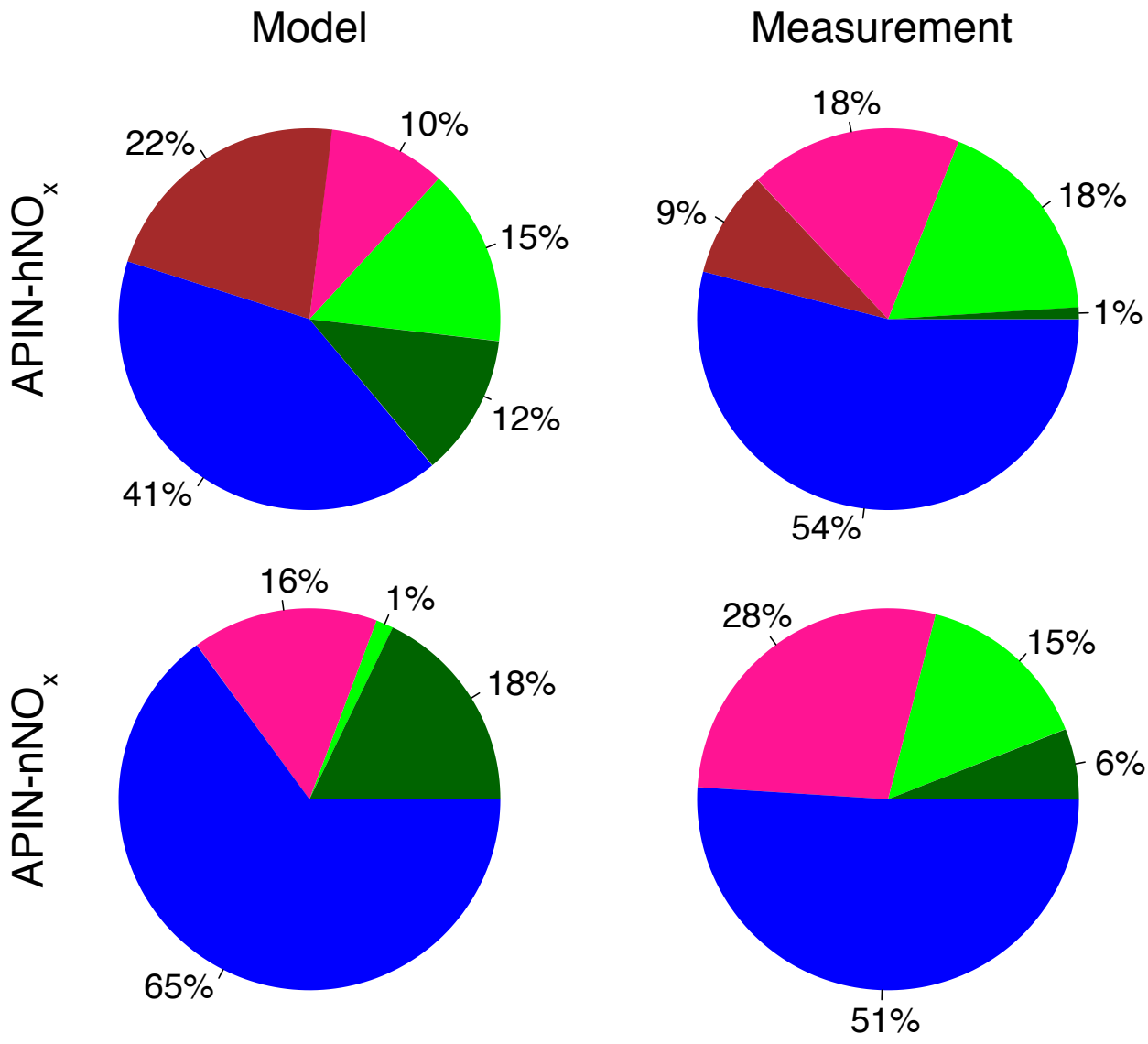

Figure S7. Relative mass abundance of measured FGs estimated by converting molar abundance of FG fragments (Figure 3) to their mass equivalents using coefficients assumed by Chhabra et al. (2011).

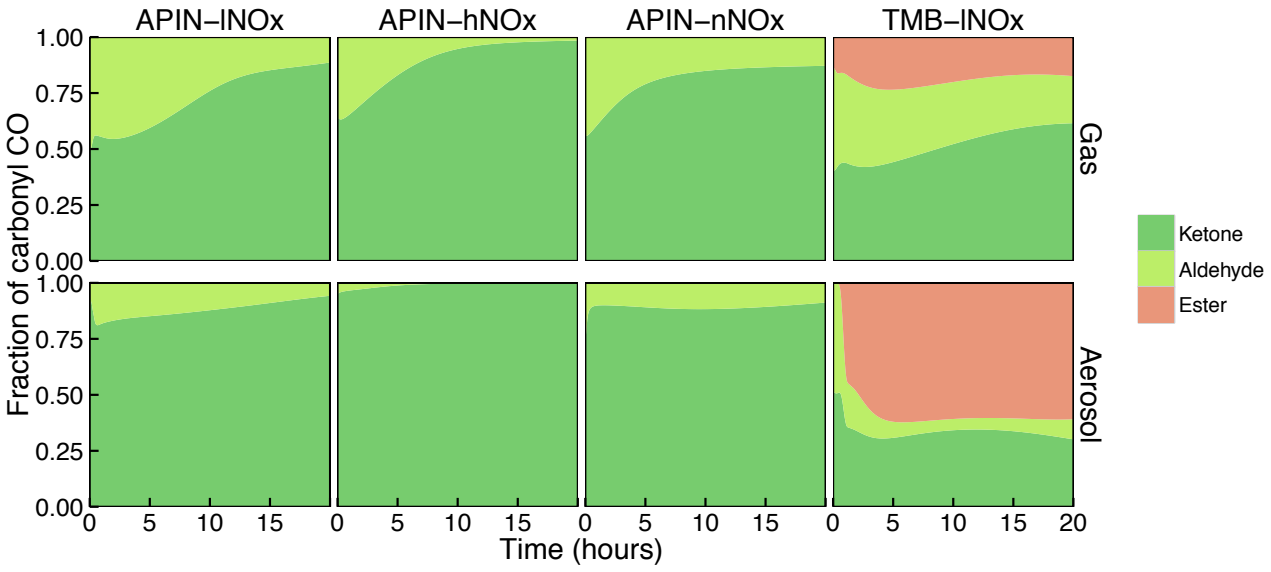

Figure S8. Fraction of carbonyl CO in each phase.

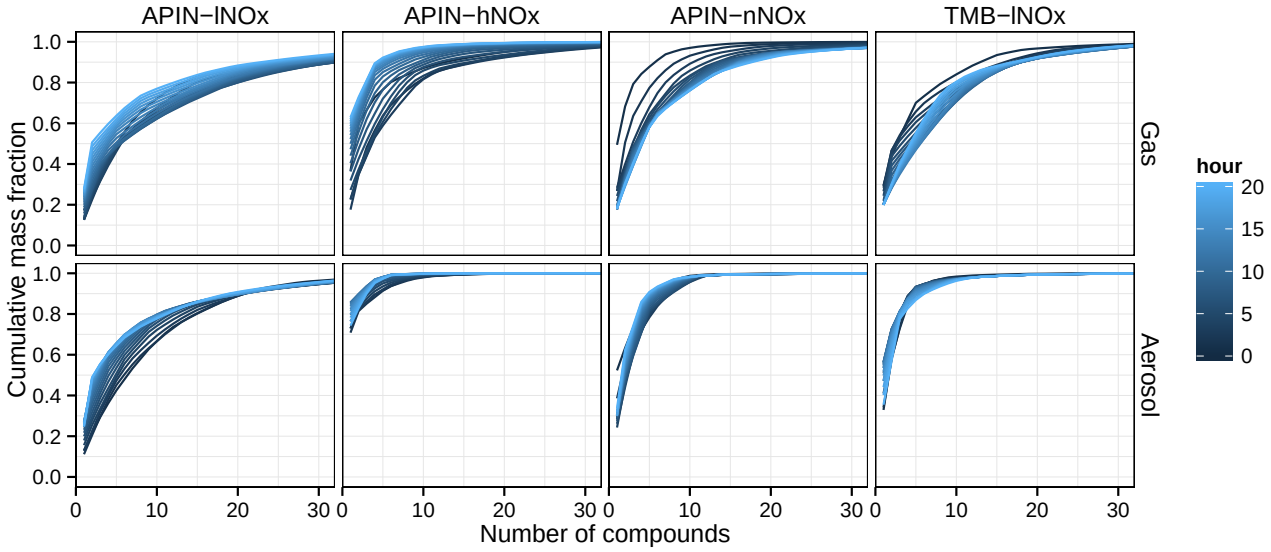

Figure S9. Cumulative mass fraction of compounds in the gas (top row) and aerosol (bottom row) phases for each simulations (shown along columns). For each phase, compounds are arranged in descending order according to their contribution (largest first).

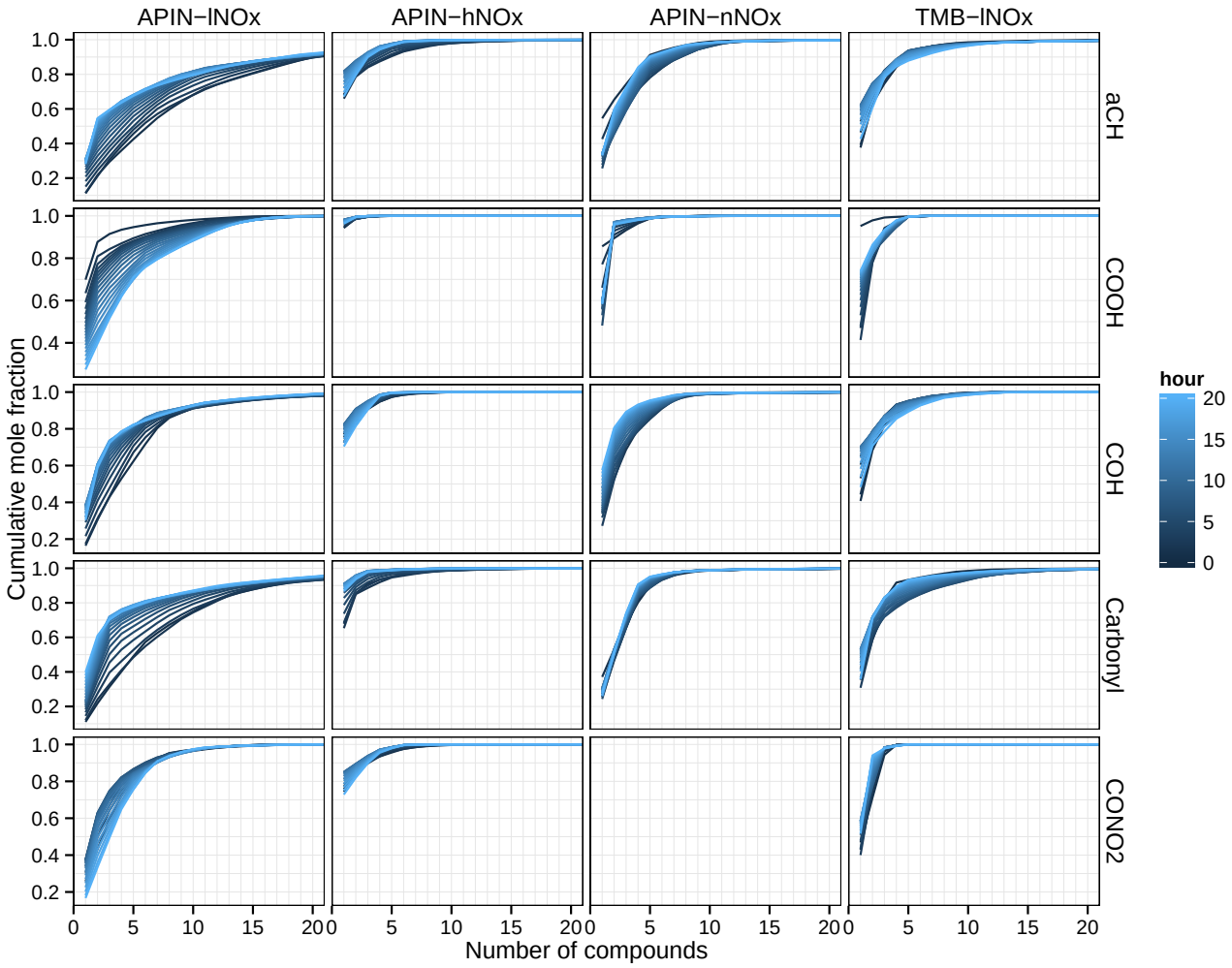

Figure S10. Cumulative fraction of compounds contributing to each FG (shown along rows) in the aerosol phase. For each FG, compounds are arranged in descending order according to their contribution (largest first). The lower bounds of y-axes on different rows are greater than zero, and are selected such that gradations in lines can be better differentiated.

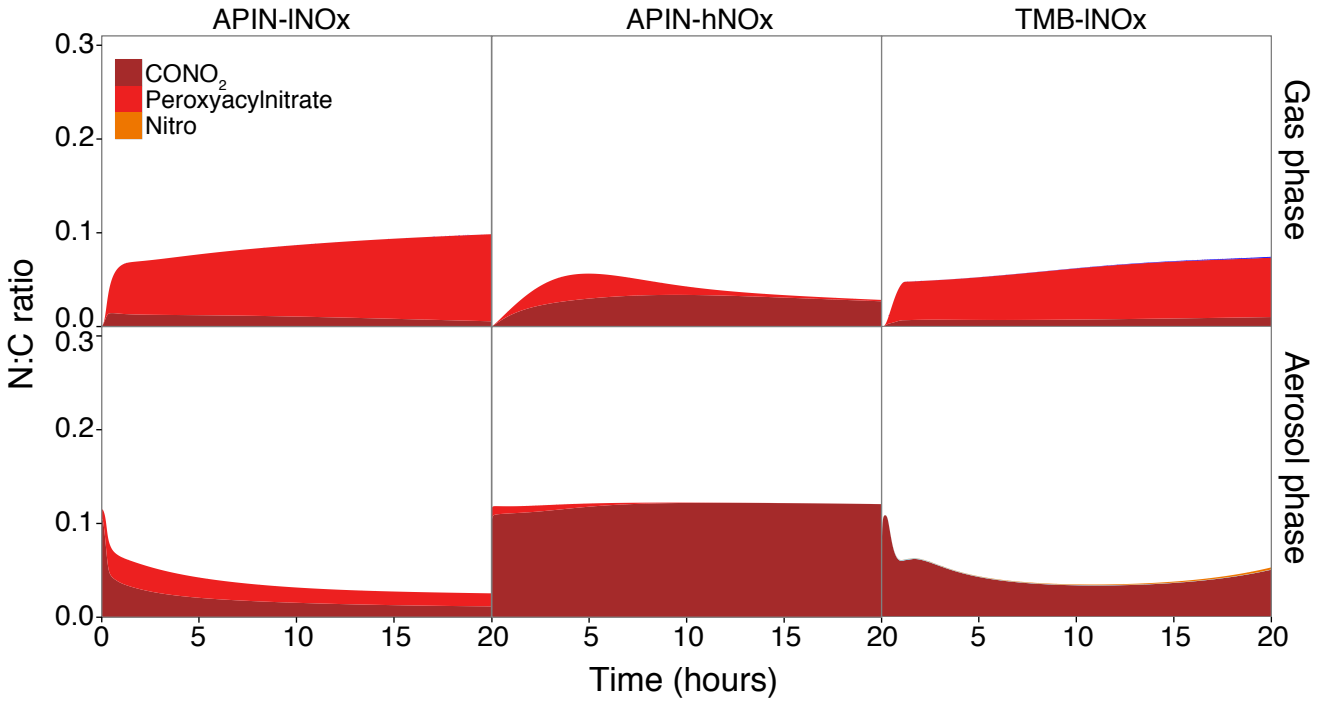

Figure S11. FGs contribution to the total N:C ratio for each simulation in which nitrogen is present. The only nitrogen containing FGs present in the system are $CONO_2$, peroxyacyl nitrate and nitro (amines and amides are not included).

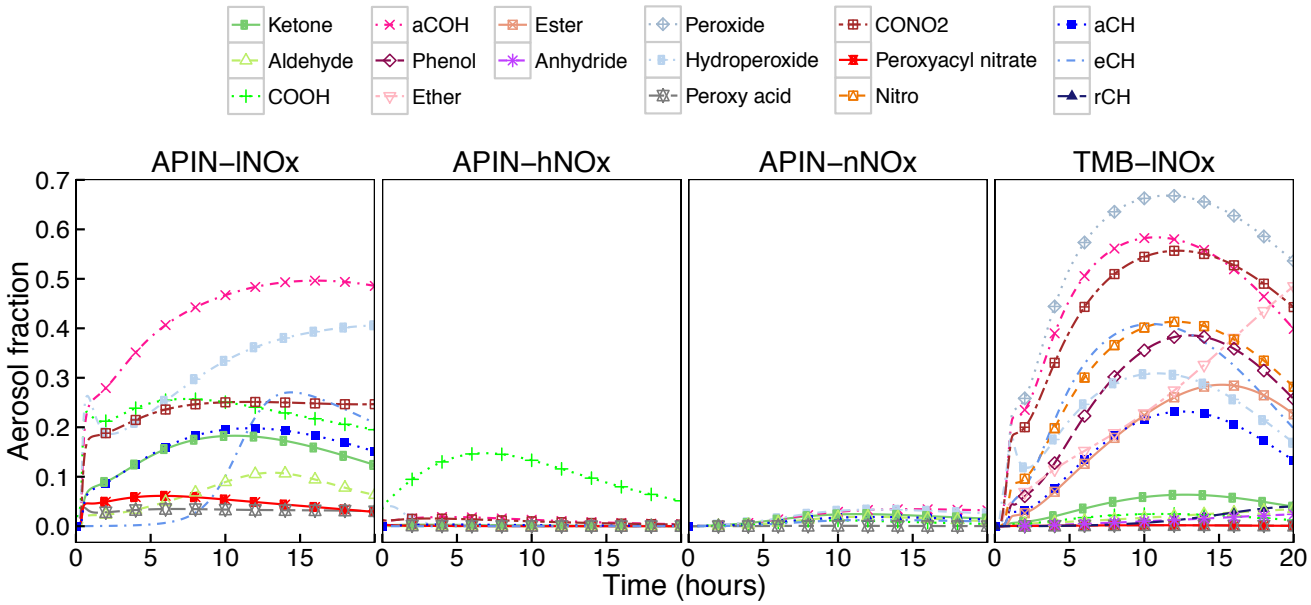

Figure S12. Evolution of aerosol fraction for each FG.

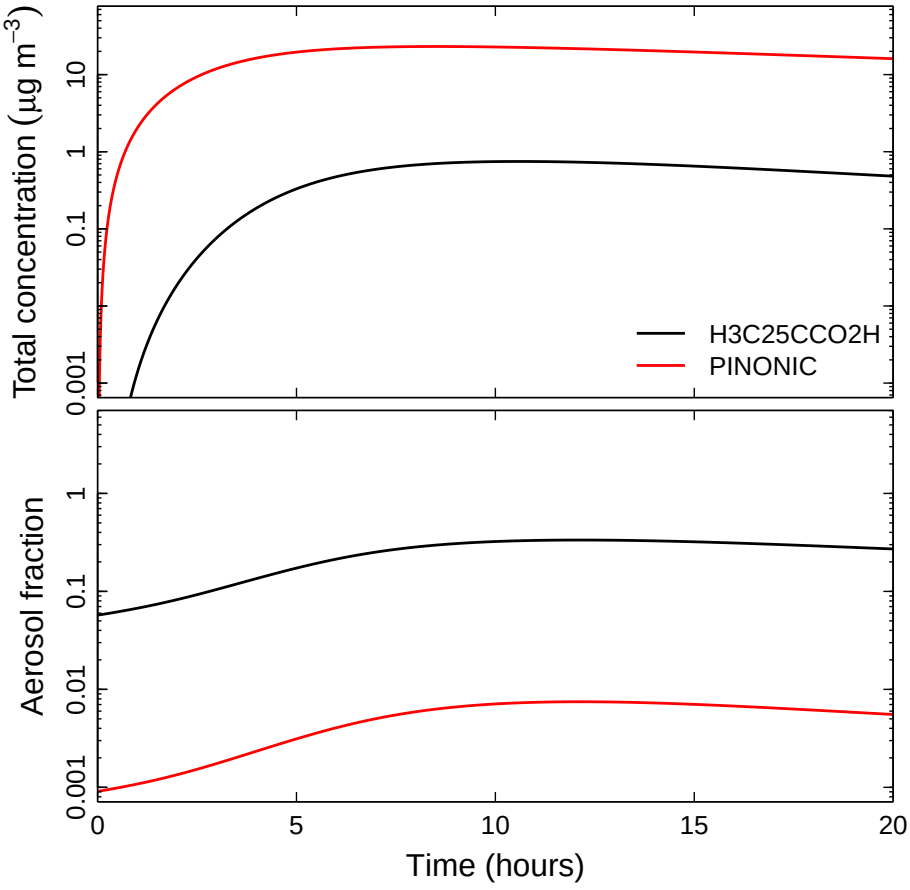

Figure S13. Total (gas+aerosol) concentrations (top) and aerosol fractions (bottom) of the two dominant acids in the APIN-nNO_x system.

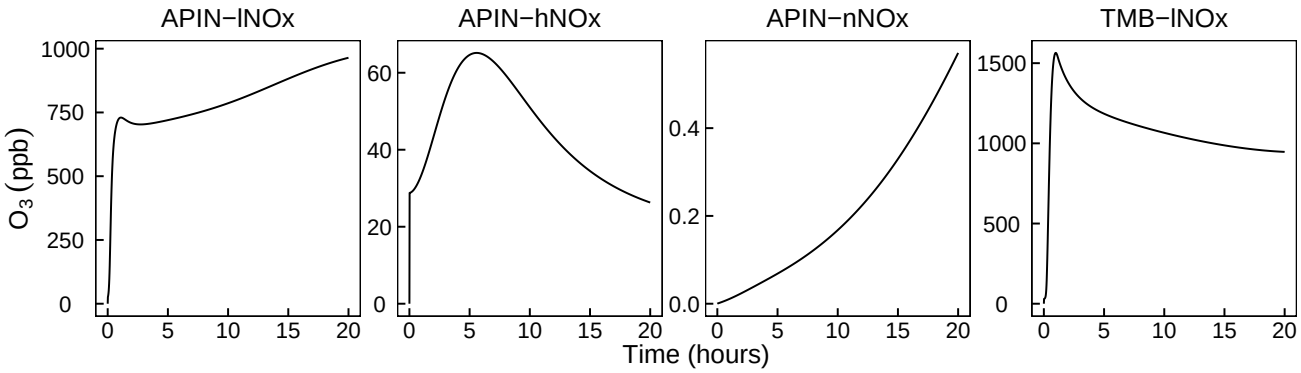

Figure S14. Time series of ozone concentrations in each of the four simulations studied.

References

Chen, Q., Liu, Y., Donahue, N. M., Shilling, J. E., and Martin, S. T.: Particle-phase chemistry of secondary organic material: modeled compared to measured O:C and H:C elemental ratios provide constraints., Environmental science & technology, 45, 4763–70, doi:10.1021/es104398s, 2011.

Chhabra, P. S., Ng, N. L., Canagaratna, M. R., Corrigan, A. L., Russell, L. M., Worsnop, D. R., Flagan, R. C., and Seinfeld, J. H.: Elemental composition and oxidation of chamber organic aerosol, Atmospheric Chemistry and Physics, 11, 8827–8845, doi:10.5194/acp-11-8827-2011, 2011.

Denbigh, K.: The Principles of Chemical Equilibrium, Cambridge University Press, Cambridge, UK, 1981.

Donahue, N. M., Robinson, A. L., Stanier, C. O., and Pandis, S. N.: Coupled partitioning, dilution, and chemical aging of semivolatile organics, Environmental Science & Technology, 40, 2635–2643, doi:10.1021/es052297c, 2006.

Donahue, N. M., Kroll, J. H., Pandis, S. N., and Robinson, A. L.: A two-dimensional volatility basis set - Part 2: Diagnostics of organic-aerosol evolution, Atmospheric Chemistry and Physics, 12, 615–634, doi:10.5194/acp-12-615-2012, 2012.

Fan, Y., Qin, F., Luo, X., Lin, L., Gui, H., and Liu, J.: Heterogeneous condensation on insoluble spherical particles: Modeling and parametric study, Chemical Engineering Science, 102, 387 – 396, doi:10.1016/j.ces.2013.08.040, 2013.

Flagan, R. C. and Seinfeld, J. H.: Fundamentals of air pollution engineering, Prentice-Hall, Inc., Englewood Cliffs, New Jersey, 1988.

Fuchs, N. A. and Sutugin, A. G.: High-Dispersed {Aerosols}, in: Topics in Current Aerosol Research, edited by Brock, G. M. and Hidy, J. R., International Reviews in Aerosol Physics and Chemistry, pp. 1–3, Pergamon, doi:10.1016/B978-0-08-016674-2.50006-6, 1971.

Grieshop, A. P., Miracolo, M. A., Donahue, N. M., and Robinson, A. L.: Constraining the Volatility Distribution and Gas-Particle Partitioning of Combustion Aerosols Using Isothermal Dilution and Thermodenuder Measurements, Environmental Science & Technology, 43, 4750–4756, doi:10.1021/es8032378, 2009.

Kostenidou, E., Pathak, R. K., and Pandis, S. N.: An algorithm for the calculation of secondary organic aerosol density combining AMS and SMPS data, Aerosol Science and Technology, 41, 1002–1010, doi:10.1080/02786820701666270, 2007.

Nguyen, T. B., Bateman, A. P., Bones, D. L., Nizkorodov, S. A., Laskin, J., and Laskin, A.: High-resolution mass spectrometry analysis of secondary organic aerosol generated by ozonolysis of isoprene, Atmospheric Environment, 44, 1032–1042, doi:10.1016/j.atmosenv.2009.12.019, 2010.

Odum, J. R., Hoffmann, T., Bowman, F., Collins, D., Flagan, R. C., and Seinfeld, J. H.: Gas/particle partitioning and secondary organic aerosol yields, Environmental Science & Technology, 30, 2580–2585, doi:10.1021/es950943+, 1996.

Pankow, J. F.: An absorption model of gas/particle partitioning of organic compounds in the atmosphere, Atmospheric Environment, 28, 185 – 188, doi:10.1016/1352-2310(94)90093-0, 1994.

Pankow, J. F.: A consideration of the role of gas/particle partitioning in the deposition of nicotine and other tobacco smoke compounds in the respiratory tract, Chemical Research In Toxicology, 14, 1465–1481, doi:10.1021/tx0100901, 2001.

Pankow, J. F.: On the ability of the gas/particle partitioning constant K(p) to consider the effects of mean MW and the presence of high MW compounds, Atmospheric Environment, 45, 1213–1216, doi:10.1016/j.atmosenv.2010.11.041, 2011.

Seinfeld, J. H. and Pandis, S. N.: Atmospheric Chemistry and Physics: From Air Pollution to Climate Change, John Wiley & Sons, New York, 2nd edition edn., 2006.

Shiraiwa, M., Berkemeier, T., Schilling-Fahnestock, K. A., Seinfeld, J. H., and Pöschl, U.: Molecular corridors and kinetic regimes in the multiphase chemical evolution of secondary organic aerosol, Atmospheric Chemistry and Physics, 14, 8323–8341, doi:10.5194/acp-14-8323-2014, 2014.